The Canadian Mineralogist
Vol. 36, pp. 1267-1283 (1998)

INTERMEDIATE SCAPOLITE: ^{29}Si MAS AND ^{27}Al SATRAS NMR SPECTROSCOPY AND RIETVELD STRUCTURE-REFINEMENT

BARBARA L. SHERRIFF[1]

Department of Geological Sciences, University of Manitoba, Winnipeg, Manitoba R3T 2N2

ELENA V. SOKOLOVA and YURII K. KABALOV

Department of Crystallography, Faculty of Geology, Moscow State University, Moscow, 119899, Russia

DAVID K. TEERTSTRA

Department of Geological Sciences, University of Manitoba, Winnipeg, Manitoba R3T 2N2

GERALD KUNATH-FANDREI, STEFFEN GOETZ and CHRISTIAN JÄGER

Institut für Optik and Quantenelektronik, Friedrich-Schiller-Universität, Max-Wien Platz 1, D- 07743 Jena, Germany

Abstract

The crystal structures of five intermediate members of the marialite (Ma) – meionite (Me) solid-solution series, with compositions ranging from Me_{15} to Me_{65} ($3.66 \leq Al \leq 4.53$ *apfu*), were examined using NMR spectroscopy and the Rietveld method of structure refinement (XRD data). ^{27}Al SATRAS and ^{29}Si MAS NMR spectra indicate that Al enters the *T*(1) site only where Al exceeds 4 *apfu*, in agreement with the structure refinement. High-resolution ^{29}Si spectra demonstrate a well-ordered structure for those samples of scapolite with 4 *apfu* Al; however, Al–Si disorder is introduced and Al–O–Al bonds are formed as the Al content becomes greater or lesser than 4 *apfu*. ^{27}Al spectra show that there is a difference in symmetry of the *T*(2) and *T*(3) sites that can be related to the adjacent alkali site containing either Ca or Na and the anion site containing Cl or CO_3. For the five scapolite samples, X-ray powder-diffraction data were analyzed in both space groups *I4/m* and $P4_2/n$, to find the most adequate model of the structure. Average interatomic distances for the tetrahedral sites indicate a difference between *T*(2) and *T*(3) for all the samples, except PAM–4. The number of weak reflections violating body-centered symmetry is constant for all the samples, except for PAM–4, which does not contain odd reflections at all. Space group *I4/m* thus is indicated for sample PAM–4, and space group $P4_2/n$ is indicated for samples TANZ, PAM–5, MAD, and MIN. There is a linear increase in the unit-cell dimension *a* from 12.04 to 12.12 Å, although *c* remains almost constant. The increase is closely related to the flexibility of *T*–O–*T* angles parallel to *a*.

Keywords: scapolite, marialite, meionite, ^{27}Al SATRAS NMR, ^{29}Si MAS NMR , Rietveld refinement, X-ray diffraction.

Sommaire

Nous avons affiné la structure cristalline de cinq membres intermédiaires de la solution solide marialite (Ma) – méionite (Me), ayant une composition comprise entre Me_{15} et Me_{65} ($3.66 \leq Al \leq 4.53$ atomes par unité formulaire) au moyen de spectres de résonance magnétique nucléaire (NMR) et d'affinements de Rietveld (données de diffraction X). Les spectres ^{27}Al SATRAS et ^{29}Si MAS montrent que l'aluminium occupe le site *T*(1) seulement dans les cas où il dépasse 4 atomes par unité formulaire, ce qui concorde avec les résultats des affinements. Des spectres ^{29}Si à haute résolution témoignent d'une structure bien ordonnée dans le cas où il y a 4 atomes d'aluminium par unité formulaire. En revanche, un désordre Al–Si et des liaisons Al–O–Al apparaissent là où la teneur en Al dépasse ou est inférieure à 4 atomes. Les spectres ^{27}Al démontrent qu'il y a une différence en symétrie des sites *T*(2) et *T*(3) selon l'occupation du site adjacent de l'ion alcalin, contenant soit Ca, soit Na, et le site de l'anion, contenant soit Cl, soit CO_3. Les cinq échantillons ont été analysés par diffraction X dans les groupes spatiaux *I4/m* et $P4_2/n$, afin de trouver le meilleur modèle de la structure. Les distances interatomiques moyennes aux tétraèdres indiquent une différence entre *T*(2) et *T*(3) dans tous les cas, sauf PAM–4. Il y a un nombre constant de réflexions de faible intensité incompatibles avec une symétrie à maille centrée dans tous les échantillons, sauf PAM–4, qui n'en montre aucune. Le groupe spatial *I4/m* est donc indiqué pour

[1] *E-mail address*: bl_sherriff@umanitoba.ca

l'échantillon PAM–4, et le groupe spatial $P4_2/n$, pour les échantillons TANZ, PAM–5, MAD, et MIN. Il y a une augmentation linéaire du paramètre réticulaire a, de 12.04 à 12.12 Å, quoique c demeure presque constant. L'augmentation est étroitement liée à la flexibilité des angles T–O–T parallèles à a.

(Traduit par la Rédaction)

Mots-clés: scapolite, marialite, méionite, ^{27}Al SATRAS NMR, ^{29}Si MAS NMR, affinement de Rietveld, diffraction X.

Introduction

Scapolite is a framework aluminosilicate with tetragonal symmetry and a general formula $M_4T_{12}O_{24}A$. Scapolite has three main forms of isomorphous substitution, Al^{3+} for Si^{4+} at the T sites, Ca^{2+} for Na^+ ($\pm K$) at the M site, and CO_3^{2-} or SO_4^{2-} for Cl^- at the A site. Concentrations of Sr, Ba or Fe are minor (with negligible Mg, Mn, Ti, P, Br or F), but A-site substitution is complicated by significant H_2O (as HCO_3, HSO_4, OH, or H_2O; Teertstra & Sherriff 1997).

Relations between the variable composition of scapolite and changes in structure, *i.e.*, phase transitions from space group $I4/m$ to $P4_2/n$ and again to $I4/m$, constitute one of the major points of discussion of the crystal chemistry of the solid solution between marialite (Ma) $Na_4Al_3Si_9O_{24}Cl$ and meionite (Me) $Ca_4Al_6Si_6O_{24}CO_3$ (Evans *et al.* 1969, Lin & Burley 1973a, Lin 1975, Lin & Burley 1973a, Teertstra & Sherriff 1996). Scapolite has long been of interest because its substitution of Ca+Al for Na+Si deviates from the $(CaAl)(NaSi)_{-1}$ plagioclase substitution. Single-crystal refinements of the structure of scapolite show that the end members of the series crystallize in space group $I4/m$ and intermediate members in $P4_2/n$ (Papike & Zoltai 1965, Papike & Stephenson 1966, Ulbrich 1973, Lin & Burley 1973a, b, *c*, 1975, Levien & Papike 1976, Peterson *et al.* 1979, Aitken *et al.* 1984, Comodi *et al.* 1990, Belokoneva *et al.* 1991, 1993). Correlation between changes in compositional trend and variation in structural parameters places the phase transitions near to Me_{15} (3.6 Al atoms per formula unit, *apfu*) and Me_{65} (4.7 Al *apfu*) [%Me = 100(Σdivalent cations)/4] (Zolotarev 1993, 1996, Teertstra & Sherriff 1996, 1997). Deviation from the plagioclase $(Ca\ Al)(Na\ Si)_{-1}$ substitution is greatest at the phase transitions, and it is likely that each portion of the series ($3 < Al < 3.6$, $3.6 \leq Al \leq 4.7$, $4.7 < Al < 6$) has its own pattern of Al–Si order.

Viewed along the c axis, the tetrahedral sites in scapolite form two types of 4-membered rings, one type consisting solely of $T(1)$ tetrahedra. In space group $I4/m$, with a 4-fold rotation axis and a center of inversion ($4_2/m$), the tetrahedra of the second type of 4-membered ring are symmetrically equivalent, so are labeled $T(2)$ (Fig. 1a), but in space group $P4_2/n$, the lack of a mirror plane m_z allows the distinction of the $T(2)$ sites into $T(2)$ and $T(3)$ (Fig. 1b). There are twice as many $T(2) + T(3)$ sites as $T(1)$ sites. Viewed along the a axis, these rings join to form 5-membered rings and large cavities, each enclosing one A anion surrounded by four M (alkali or alkaline earth) cations.

Here, we examine the intermediate portion of the series, with $P4_2/n$ symmetry, for which X-ray powder-diffraction patterns show reflections violating body-

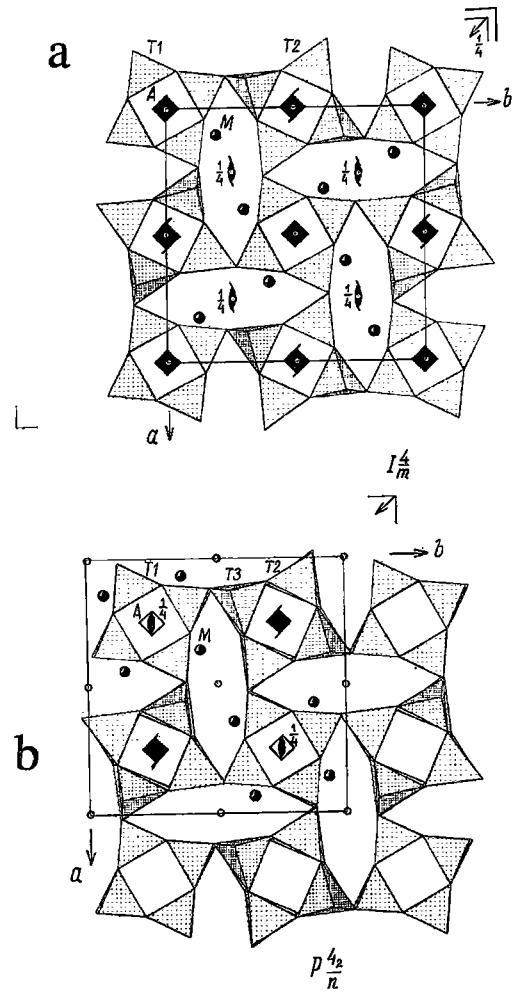

FIG. 1. Scapolite structure. Projection xy: a) space group $I4/m$, b) space group $P4_2/n$. Symmetry elements are indicated to emphasize the difference between T sites in both space groups.

centered symmetry, peaking in intensity near Me_{37} (Lin & Burley 1973b). Structure refinement using X-ray-diffraction data suggests a highly ordered Al–Si distribution between the tetrahedral framework sites $T(2)$ and $T(3)$ at a composition near Me_{37} ($Al_4Si_8O_{24}$), which has a Si:Al ratio of 2:1 (Lin 1975). Magic-angle spinning nuclear magnetic resonance (MAS NMR) spectroscopy also indicates a highly ordered state near this composition (Sherriff *et al.* 1987). However, on a local scale of several unit cells, the symmetry may be modified. Hassan & Buseck (1988) found that space groups $P4_2/m$ or $P4$ were valid for the intermediate compositions of scapolite on the basis of HRTEM data for one sample. This finding was suggested to result from order of Cl and CO_3 on the anion site.

In view of the complex substitutions possible in scapolite, crystal-chemical models of the structure have to be based on techniques for studying both long-range and short-range atomic order. Therefore we are studying the entire scapolite series using both Rietveld structure refinement of powder X-ray-diffraction data and both MAS and satellite transition (SATRAS) NMR, which gives considerably improved resolution of ^{27}Al spectra. In the first paper in this series (Sokolova *et al.* 1996), we examined part of the marialitic isomorphous series and found a linear trend in the cell parameters from XRD data; also, we found evidence from NMR spectroscopy for the presence of Al–O–Al bonds despite the low Al content of these samples of scapolite and contrary to Lowenstein's Rule (Lowenstein 1954). In this paper, we investigate the structure and cation order of an intermediate isomorphous series of scapolite compositions with $3.6 \leq Al \leq 4.7$ and a meionite content between 15% and 65% using the same techniques of Rietveld structure refinement of X-ray diffraction data and NMR spectroscopy.

Experimental Procedures

Materials

The scapolite samples in this study are named after their geological occurrence. Some of our samples were donated as fine-grained mineral separates. Polished thin sections were prepared for all samples. Associated phases were identified by a combination of optical microscopy, electron-microprobe (EMP) analysis, and X-ray powder diffraction. PAM–4, PAM–5 and PAM–22 are from the Kukurt gem scapolite deposit, eastern Pamir, Tajikistan. The geological position and mineralogy of the Kukurt deposit have been discussed previously (Sokolova *et al.* 1996, Zolotarev 1993). PAM–4, PAM–5 and PAM–22 crystals are of gem quality, and transparent. The crystals are euhedral with a prismatic habit. The dimensions of the crystals vary from 0.5 to 3 cm along the *c* axis.

TANZ is from a granulite near Morongoro, Tanzania (Zwaan 1971, Smetzer *et al.* 1976, Coolen 1980, Hoefs *et al.* 1981, Jones *et al.* 1983). Chemical composition was determined from electron-microprobe data by Moecher (1988) and also by Teertstra & Sherriff (1996, 1997). Our powdered sample contains trace quantities of calcite and albite.

CA63A is a separate of coarse bladed yellow-green scapolite crystals, altered along the grain margins, from a zoned skarn at Grand Calumet Township, Quebec (24 km south of Gib Lake; Shaw *et al.* 1965). Results of wet-chemical and EMP analyses are given in Evans *et al.* (1969). Our sample contains traces of quartz, calcite, amphibole and K-feldspar ($Kfs_{85.7}An_{11.9}Ab_{2.4}$). Chemical composition was determined from EMP data by Teertstra & Sherriff (1996, 1997).

MAD is a transparent yellow gem scapolite from Madagascar. EMP data are given in Moecher (1988) and also by Teertstra & Sherriff (1996, 1997). Our sample contains traces of calcite.

MIN is from a skarn near Minden, Ontario. EMP data are given in Moecher (1988) and also by Teertstra & Sherriff (1997). Our sample contains minor K-feldspar.

Chemical analyses

Chemical analyses were made using a CAMECA SX–50 electron microprobe operating at 15 kV and 20 nA, with a beam diameter of 10 μm and count times of 20 s. Data were reduced using the "PAP" procedure of Pouchou & Pichoir (1985). We used as principal reference standards gem-quality meionite from Brazil, U.S.N.M. #R6600–1 (Dunn *et al.* 1978), albite from the Rutherford mine, Amelia Courthouse, Virginia, U.S.A., anorthite from Sitkin Island, and tugtupite from the type locality in southern Greenland (R.O.M. #M32790). The elements Mn, Mg, Ti, P, Br and F were sought, but not detected. Absolute quantities of H_2O were determined at 900°C by Karl Fischer titration using a Mitsubishi moisture meter. Prior to the determination, the finely ground samples were dried at 110°C to remove any surficial water. Formulae were calculated using the method of Teertstra & Sherriff (1996, 1997). The results of chemical analysis and formula calculations are given in Table 1.

Rietveld structure refinement

X-ray powder-diffraction patterns of the scapolite samples were collected on an ADP–2 diffractometer using Cu$K\alpha$ radiation (Ni-filtered) over the range $9° < 2\theta < 150°$, with a step width of 0.02° 2θ and a count time of 5 s per step. Most of the samples are pure; except for two samples, peaks of phases associated with scapolite are of low intensity and do not overlap with diffraction maxima of scapolite.

Structure refinements were carried out with the Wyriet, version 3.3 program (Schneider 1989). The atomic coordinates of Sokolova *et al.* (1996) for $Me_{7.6}$ (PAM–3) with a space group of $I4/m$ and the atomic

TABLE 1. COMPOSITION OF INTERMEDIATE MEMBERS OF THE MARIALITE – MEIONITE SERIES

	PAM-4	PAM-22	TANZ*	PAM-5	CA63A*	MAD*	MIN*
SiO_2 (wt. %)	57.74	57.53	55.15	54.76	53.88	51.48	48.98
Al_2O_3	21.49	21.71	21.96	22.33	22.81	23.90	25.24
Fe_2O_3	0.08	0.04	0.12	0.00	0.11	0.01	0.00
Na_2O	11.10	9.99	9.17	8.42	8.26	6.86	5.17
K_2O	0.29	1.10	1.30	1.04	1.42	0.50	0.72
CaO	5.38	5.99	6.94	8.41	8.32	11.34	13.72
SrO	0.07	0.09	0.07	0.17	0.28	0.10	0.29
BaO	0.08	0.00	0.03	0.12	0.02	0.04	0.02
Cl	3.41	3.34	2.99	2.30	2.75	1.84	1.10
F	0.00	0.00	0.03	0.00	0.15	0.05	0.14
SO_3	0.27	0.08	0.86	1.16	0.17	0.81	1.41
CO_2	n.d.	n.d.	1.14	n.d.	n.d.	2.18	2.74
H_2O	0.16	0.20	0.14	0.05	0.20	0.14	0.18
Sum	100.08	99.86	99.93	98.77	98.38	99.41	99.75
O=Cl,F	–0.78	–0.74	–0.69	–0.52	–0.68	–0.43	–0.31
Total	99.30	99.12	99.24	98.25	97.70	99.98	99.44
Si (*apfu*)	8.34	8.31	8.16	8.11	8.01	7.76	7.48
Al	3.66	3.69	3.83	3.90	3.99	4.24	4.53
Fe^{3+}	0.09	0.00	0.00	0.00	0.00	0.00	0.00
Na	3.11	2.98	2.63	2.42	2.38	2.00	1.53
K	0.05	0.20	0.25	0.20	0.27	0.10	0.14
Ca	0.83	0.93	1.10	1.33	1.33	1.83	2.24
Fe^{2+}	0.00	0.00	0.01	0.00	0.01	0.01	0.00
Cl	0.84	0.82	0.70	0.58	0.69	0.47	0.28
F	0.00	0.01	0.01	0.00	0.07	0.02	0.07
S	0.03	0.19	0.10	0.13	0.02	0.09	0.57
H^+	0.00	0.00	0.14	0.00	0.00	0.08	0.02
OH^-	0.15	0.19	0.00	0.02	0.00	0.00	0.00
H_2O	0.00	0.00	0.00	0.00	0.10	0.03	0.00
Si/Al	2.28	2.25	2.13	2.08	2.00	1.83	1.65
%Me	21.2	23.3	27.9	33.6	33.6	46.7	56.3

The proportions of H^+, OH, H_2O, Fe^{3+} and Fe^{2+} were calculated as described in the text. n.d.: not determined. *Teertstra & Sherriff (1996, 1997).

coordinates of Aitken *et al.* (1984) for synthetic meionite with a space group of $P4_2/n$ were used as a starting model for the refinement. The structures of five samples of scapolite were refined in space group of $P4_2/n$ as well as $I4/m$. Three mixing parameters were refined for the Pearson profile function (6 FWHM) using scattering factors for ionized species and a graphically modeled background using a polynomial with five refined variables. The total number of refined parameters including cell parameters, zero point, sample displacement, asymmetry ($2\theta < 40°$), preferred orientation, atomic coordinates, isotropic temperature-factors, site occupancies for *M* site, *etc.* varied from 80 (space group $I4/m$) to 100 (space group $P4_2/n$).

The refinement of cation populations at the *M* site is complicated by the presence of three cations with similar values of scattering factor: Na^+ ($Z = 11$), Ca^{2+} ($Z = 20$), and K^+ ($Z = 19$). To check the accuracy of the Rietveld refinement, the fraction of K was fixed according to the analytical results, and the populations of Na and Ca refined for comparison with the electron-microprobe analytical results. Atomic parameters for the *T* site were refined using a Si^{4+} scattering factor, which is nearly identical to the Al^{3+} scattering factor.

To complete the structure model for intermediate scapolite, additional atoms of C, S and the oxygen atoms of the carbonate group O(7), O(8), and O(9) and of the sulfate tetrahedron O(10) were included in the refinement. The atomic coordinates of C, S, O(7), O(8), O(9), and O(10) were fixed at values taken from Aitken *et al.* (1984) for Me_{84} scapolite (carbonate group) and Peterson *et al.* (1979) for Me_{70} scapolite (sulfate group). The partial occupancy of all the oxygen sites corresponding to the disordered carbonate and sulfate groups would give unreasonable Rietveld refinement of temperature factors. Therefore, in the *A* site, temperature factors were calculated both for Cl and S atoms, but fixed at 3.5 $Å^2$ for C, O(7), O(8), O(9), and O(10). The C atom is shifted from the *A* site and, together with oxygen atoms O(7), O(8) and O(9), constitute the CO_3 triangle. Site occupancies of the atoms other than Cl in the *A* site were fixed at the values obtained from the calculations of stoichiometric formula.

After the refinements, difference-Fourier maps D(xyz) were examined for additional intensity, which might represent additional positions for volatile species in the structure.

Observed and calculated structure-factors may be obtained from the Depository of Unpublished Data, CISTI, National Research Council, Ottawa, Ontario K1A 0S2.

Nuclear magnetic resonance spectroscopy

^{27}Al MAS NMR spectra were obtained on a Bruker AMX 400, at the Institut für Optik and Quantenelektronik, Friedrich-Schiller-Universität, Jena, Germany, at a frequency of 104.2 MHz. Rotation rates of 14 kHz were obtained using a Bruker high-speed probe, spinning within an accuracy of ±3 Hz. A solid π-pulse for PAM–1 of 8 μs was determined, and a 1 μs pulse used for all samples in conjunction with a 0.2 s recycle delay. It was considered very important for comparison of the spectra that the data for each sample be obtained with identical experimental parameter setup and probehead configurations. Therefore, it was decided to use the spectra of samples PAM–22 and CA63A instead of PAM–4 and PAM–5 because the data for PAM–4 and PAM–5 were acquired on a different day and thus the tuning state of the spectrometer and probe was not exactly repeatable. PAM–22 and CA63A have similar Al contents as PAM–4 and PAM–5, respectively. Twenty thousand scans were accumulated for PAM22, CA63A, MAD and MIN, and 12500 scans for TANZ. The baseline roll after phasing caused by the finite pulse-length and dead-time was corrected using the cubic spline fit in the spectrometer software. The spectra were referenced to an aqueous solution of $AlCl_3$. Simulations of the satellite transitions, including a distribution of the quadrupole parameters (Kunath *et al.* 1992), were performed on a Pentium processor using the theory of Skibsted *et al.* (1991).

^{29}Si spectra were recorded on the AMX500 with a Doty MAS probe at the Prairie Regional NMR Centre, Winnipeg, Manitoba, at a frequency of 99.36 MHz, with a recycle delay of 5 s, and referenced to ^{29}Si in tetramethylsilane (TMS). The number of Si atoms corresponding to each *T*-site environment was calculated from the relative intensities of the ^{29}Si peaks of computer simulations using a least-squares iterative process, which varied the isotropic chemical shift, the Gaussian and Lorentzian broadening parameters, and the intensity of each line. A range of recycle delays were explored for both ^{29}Si and ^{27}Al to ensure complete relaxation for the values chosen.

Results and Discussion

Structure refinement

Rietveld refinements were done for each sample in space groups *I4/m* and $P4_2/n$. Based on interatomic distances at the *T* sites, space group *I4/m* was found to be preferable for PAM–4, and $P4_2/n$, for samples TANZ, PAM–5, MAD and MIN. The final agreement indices for both space groups, *I4/m* and $P4_2/n$, are very similar, which is not surprising as space group $P4_2/n$ is a subgroup of a space group *I4/m*. The profile agreement indices (R_p and R_{wp}) are similar, but the R_F values, which are analogous to single-crystal *R*-factors, are actually lower in space group *I4/m*, with values of 3.44 – 5.50, in contrast to values of 4.86 – 7.60 in space group $P4_2/n$. The number of reflections with $h + k + l \neq 2n$ violating the body-centered lattice is the same for samples TANZ, PAM–5, MAD and MIN and constitutes 46% of the total number of reflections in space group $P4_2/n$. These reflections are weak and comparable with a background level; therefore, powder patterns calculated in different space-groups are similar.

Cell parameters, pattern parameters and agreement indices for the Rietveld refinement in space group $P4_2/n$ are given in Table 2. Atomic coordinates and isotropic temperature-factors are given in Table 3, and selected interatomic distances and angles, in Table 4. Tables 2, 3 and 4 also contain the data from a refinement in space group *I4/m* for PAM–4.

Atomic coordinates and isotropic temperature-factors do not show significant differences between the two space groups (PAM–4, Table 3), although the quotation of the average interatomic bond-distances to three decimal places for space group *I4/m* compared to two for space group $P4_2/n$ (PAM–4, Table 4) indicates the higher degree of precision for the Rietveld structural refinement in space group *I4/m*. The average <*T*(1)–O> bonds for PAM–4, TANZ, PAM–5, MAD and MIN are 1.61, 1.60. 1.61, 1.62 and 1.63 Å (Table 4), indicating that the *T*(1) site is occupied by Si in samples from PAM–4, TANZ and PAM–5, which all have Al content ≥3.66 *apfu*. The longer <*T*(1)–O> bond lengths for MAD and MIN are indicative of Al entering the *T*(1) site where the Al content becomes greater than 4, with the *T*(1) site of MIN containing more Al than that of MAD.

Differences of 0.10, 0.09 and 0.10 Å, respectively, were found between <*T*(2)–O> and <*T*(3)–O> distances for TANZ, PAM–5 and MAD (Al content: 3.83, 3.90 and 4.24 *apfu*; Table 4), indicating that for these compositions, Si and Al are ordered between the *T*(2) and *T*(3) sites. Where the Al content becomes greater than 4 *apfu* and Al enters the *T*(1) site, it becomes impossible to avoid all Al–O–Al bonds. Si and Al then become more evenly distributed between the *T*(2) and *T*(3) sites, and the difference between <*T*(2)–O> and <*T*(3)–O> bond distances decreases to 0.5 Å for MIN (4.53 *apfu* Al).

The average <*M* – O> distances decrease slightly with meionite content, from 2.72 Å for PAM–4 to 2.68 Å for MIN (Table 4). This distance can be related to the occupation of the *M* site by Ca, K or Na. The effective ionic radii of Na^+, K^+, and Ca^{2+} in eightfold coordination are 1.16, 1.3, and 1.12 Å respectively (Shannon & Prewitt 1969). Therefore, the general decrease in <*M*–O> distance with increasing meionite content is due to the replacement of Na^+ by Ca^{2+} (Table 1). The slightly larger values of <*M*–O> distance for TANZ of 2.73 Å is due to the higher K content of this sample of scapolite (Table 1). As <*M*–O> bond lengths decrease with Al content, the <*M*–*A*> distance increases. In intermediate-range scapolite, the *A* site is occupied by Cl and S, whereas C is shifted from the *A* site. The distances in the CO_3 and SO_4 group are within standard values using

TABLE 2. CELL PARAMETERS, PATTERN PARAMETERS AND AGREEMENT INDICES FROM RIETVELD REFINEMENT

	PAM-4	PAM-4	TANZ	PAM-5	MAD	MIN
S.G.	*I4/m*	$P4_2/n$	$P4_2/n$	$P4_2/n$	$P4_2/n$	$P4_2/n$
a (Å)	12.0415(1)	12.0416(1)	12.0642(1)	12.0739(1)	12.0957(1)	12.1224(1)
c (Å)	7.5809(1)	7.5810(1)	7.5796(1)	7.5806(1)	7.5730(1)	7.5110(1)
V (Å^3)	1099.22(1)	1099.25(1)	1103.17(1)	1105.09(1)	1107.97(1)	1103.76(1)
2θ range	12–150°	2–150°	12–150°	9.6–129°	12–150°	12–150°
No. refl.	1225	2265	2276	1851	2286	2288
R_p[1]	4.09	3.99	3.90	3.85	4.62	4.45
R_{wp}[2]	5.34	5.19	4.99	6.48	6.03	5.80
R_{exp}[3]	4.74	4.63	4.51	5.05	4.98	5.04
R_B[4]	2.24	2.57	3.90	2.78	3.52	3.91
R_F[5]	3.44	5.05	7.60	4.86	6.00	5.86
s[6]	1.13	1.11	1.10	1.27	1.21	1.15
DWD[7]	1.71	1.75	1.70	1.37	1.53	1.62
s_x[8]	1.436	1.400	1.487	1.627	1.524	1.446

(1) R_p: pattern *R* factor. (2) R_{wp}: weighted pattern *R*-factor. (3) R_{exp}: expected value of R_{wp}. (4) R_B: Bragg *R*-factor (*R*-value for Bragg intensities). (5) R_F: *R*-value based on the observed and calculated structure-amplitudes. (6) $s = R_{wp}/R_{exp}$. (7) *DWD*: Durbin–Watson *d* statistic (Hill & Flack 1987). (8) s_x: multiplication factor for all e.s.d's according to Bérar & Lelann (1991). S.G.: space group. No. Refl.: number of reflections. Origin of $P4_2/n$ setting: $\bar{4}$.

TABLE 3. ATOMIC COORDINATES AND B-FACTORS (Å²)

		PAM-4	PAM-4	TANZ	PAM-5	MAD	MIN
space group		*I4/m*	$P4_2/n$	$P4_2/n$	$P4_2/n$	$P4_2/n$	$P4_2/n$
M	*x*	0.3688(4)	0.5404(6)	0.5397(7)	0.5387(6)	0.5353(6)	0.5357(4)
	y	0.2903(6)	0.6191(4)	0.6183(6)	0.6163(5)	0.6112(5)	0.6111(4)
	z	0.5	0.752(6)	0.741(3)	0.745(3)	0.745(3)	0.745(3)
	B_{iso}	3.1(2)	1.2(1)	4.0(1)	3.5(1)	2.3(1)	2.38(8)
T(1)	*x*	0.3394(4)	0.6598(3)	0.6598(5)	0.6605(5)	0.6598(5)	0.6601(4)
	y	0.4097(3)	0.5899(4)	0.5904(6)	0.5897(5)	0.5887(5)	0.5892(4)
	z	0	0.250(3)	0.248(3)	0.250(3)	0.250(5)	0.249(1)
	B_{iso}	1.1(1)	1.2(2)	1.83(7)	1.85(7)	1.2(1)	1.42(8)
T(2)	*x*	0.6616(3)	0.165(1)	0.164(2)	0.164(2)	0.164(2)	0.164(2)
	y	0.9113(3)	0.912(1)	0.913(2)	0.912(2)	0.911(2)	0.910(1)
	z	0.7941(3)	0.044(1)	0.040(2)	0.043(2)	0.040(2)	0.046(1)
	B_{iso}	1.87(9)	1.6(1)	1.9(3)	1.7(5)	1.9(5)	2.03(3)
T(3)	*x*		0.089(1)	0.088(2)	0.089(2)	0.092(2)	0.090(1)
	y		0.664(1)	0.665(2)	0.663(2)	0.663(2)	0.664(1)
	z		0.957(3)	0.955(2)	0.956(2)	0.954(3)	0.959(1)
	B_{iso}		2.1(1)	1.7(3)	1.8(5)	1.7(5)	1.0(5)
O(1)	*x*	0.4572(7)	0.6017(7)	0.6023(7)	0.6045(6)	0.6023(9)	0.6009(9)
	y	0.3520(7)	0.7072(7)	0.7062(9)	0.7067(7)	0.7058(9)	0.7068(6)
	z	0	0.255(7)	0.254(6)	0.249(5)	0.248(5)	0.250(3)
	B_{iso}	1.6(2)	1.8(1)	2.0(3)	1.8(5)	1.9(3)	2.1(3)
O(2)	*x*	0.6914(7)	0.1280(7)	0.1264(9)	0.1275(8)	0.1235(9)	0.1246(7)
	y	0.8780(7)	0.9417(7)	0.943(1)	0.941(1)	0.9388(9)	0.9379(6)
	z	0	0.249(7)	0.255(6)	0.257(6)	0.240(6)	0.246(5)
	B_{iso}	1.7(2)	1.9(2)	2.6(3)	2.4(3)	2.1(3)	1.1(3)
O(3)	*x*	0.3497(6)	0.199(4)	0.194(3)	0.195(3)	0.206(3)	0.207(1)
	y	0.9490(6)	0.597(3)	0.607(3)	0.603(3)	0.601(3)	0.599(3)
	z	0.7831(7)	0.030(6)	0.039(6)	0.041(5)	0.036(5)	0.044(5)
	B_{iso}	1.8(2)	2.0(3)	2.2(6)	2.3(7)	1.9(6)	1.5(5)
O(4)	*x*	0.2725(4)	0.102(3)	0.097(3)	0.097(3)	0.101(3)	0.105(3)
	y	0.3708(4)	0.802(3)	0.797(3)	0.797(3)	0.808(3)	0.808(1)
	z	0.8241(8)	0.963(6)	0.965(6)	0.964(5)	0.956(5)	0.956(3)
	B_{iso}	2.0(2)	1.7(3)	2.1(6)	2.0(6)	2.7(8)	2.3(5)
O(5)	*x*		0.621(3)	0.623(3)	0.620(3)	0.624(3)	0.624(3)
	y		0.525(3)	0.523(3)	0.523(3)	0.523(3)	0.523(3)
	z		0.071(6)	0.083(5)	0.079(3)	0.070(5)	0.066(3)
	B_{iso}		1.7(3)	2.0(5)	1.3(7)	2.1(1)	2.5(6)
O(6)	*x*		0.980(3)	0.977(3)	0.978(3)	0.978(3)	0.982(1)
	y		0.620(3)	0.624(3)	0.623(3)	0.617(3)	0.617(3)
	z		0.076(6)	0.069(5)	0.070(3)	0.078(5)	0.080(3)
	B_{iso}		2.6(3)	3.4(6)	3.1(6)	2.0(1)	1.1(5)
A^1	*x*	0.5	0.25	0.25	0.25	0.25	0.25
	y	0.5	0.25	0.25	0.25	0.25	0.25
	z	0.5	0.25	0.25	0.25	0.25	0.25
	B_{iso}	6.1(5)	6.6(3)	6.4(3)	7.0(3)	4.5(6)	3.2(5)

(1) PAM-4, space group *I4/m*: Cl and S atoms were put in the site *A* (½ ½ ½). Simultaneously, C (x = 0.509, y = 0.481, z = 0.5), O(7) (x = 0.517, y = 0.376, z = 0.5), O(8) (x = 0.596, y = 0.540, z = 0.5), O(9) (x = 0.414, y = 0.526, z = 0.5), O(10) (x = 0.600, y = 0.518, z = 0.606) were added to the structure model. C, O(7) - O(9) constitute CO_3 triangle, S and O(10) form SO_4 tetrahedron. For the C, O(7), O(8), O(9), O(10) coordinates *x, y, z* and temperature factor B_{iso} = 3.5 Å² were fixed.
(2) Space group $P4_2/n$: Cl and S atoms were put in the site *A* (¼ ¼ ¼). Simultaneously, C (x = 0.259, y = 0.231, z = 0.250), O(7) (x = 0.126, y = 0.267, z = 0.250), O(8) (x = 0.290, y = 0.346, z = 0.250), O(9) (x = 0.276, y = 0.164, z = 0.250), O(10) (x = 0.268, y = 0.350, z = 0.356) were added to the structure model. C, O(7) - O(9) constitute CO_3 triangle, S and O(10) form SO_4 tetrahedron. For the C, O(7), O(8), O(9), O(10) coordinates *x, y, z* and temperature factor B_{iso} = 3.5 Å² were fixed. The atomic coordinates of C, O(7), O(8), O(9) (Aitken *et al.* 1984) and O(10) (Peterson *et al.* 1979) were converted because there is another origin in space group $P4_2/n$ relative to that in space group *I4/m*.

TABLE 4. SELECTED INTERATOMIC DISTANCES (Å) AND ANGLES(°), SAMPLES OF INTERMEDIATE SCAPOLITE

	PAM-4		PAM-4	TANZ	PAM-5	MAD	MIN
space group	*I4/m*		$P4_2/n$	$P4_2/n$	$P4_2/n$	$P4_2/n$	$P4_2/n$
T(1) - O(1)	1.580(7)	*T*(1) - O(1)	1.576(7)	1.560(8)	1.566(7)	1.578(8)	1.596(8)
T(1) - O(1)'	1.610(6)	*T*(1) - O(1)'	1.609(7)	1.624(8)	1.613(7)	1.634(8)	1.620(8)
T(1) - O(4)	1.627(5)	*T*(1) - O(5)	1.63(3)	1.56(3)	1.60(2)	1.64(3)	1.67(2)
T(1) - O(4)	1.627(5)	*T*(1) - O(6)	1.64(3)	1.66(3)	1.65(2)	1.62(3)	1.64(2)
<*T*(1) - O>	1.611		1.61	1.60	1.61	1.62	1.63
O(1)-*T*(1)-O(1)'	110.7(4)	O(1)-*T*(1)-O(1)'	111.3(4)	111.3(4)	109.2(3)	110.4(4)	111.7(4)
O(1)-*T*(1)-O(4)	108.5(2)	O(1)-*T*(1)-O(5)	109(2)	109(1)	109(1)	108(1)	108(1)
O(1)-*T*(1)-O(4)	108.5(2)	O(1)-*T*(1)-O(6)'	108(2)	110(1)	109(1)	108(1)	109(1)
O(1)'-*T*(1)-O(4)'	109.5(2)	O(1)'-*T*(1)-O(5)	108(2)	111(1)	111(1)	109(1)	108(1)
O(1)'-*T*(1)-O(4)'	109.5(2)	O(1)'-*T*(1)-O(6)	111(2)	106(1)	109(1)	111(1)	111(1)
O(4)-*T*(1)-O(4)'	110.1(3)	O(5)-*T*(1)-O(6)	110(2)	107(1)	110(1)	110(1)	108(8)
<O-*T*(1)-O>	109.5		110	109	110	109	109
T(2) - O(2)	1.660(3)	*T*(2) - O(2)	1.65(4)	1.73(3)	1.72(3)	1.62(3)	1.75(2)
T(2) - O(3)	1.654(5)	*T*(2) - O(3)	1.65(3)	1.73(3)	1.72(2)	1.59(2)	1.75(2)
T(2) - O(3)'	1.650(5)	*T*(2) - O(4)	1.65(3)	1.71(3)	1.71(2)	1.60(2)	1.58(2)
T(2) - O(4)	1.691(4)	*T*(2) - O(5)	1.71(3)	1.71(3)	1.71(2)	1.66(3)	1.68(2)
<*T*(2) - O>	1.664		1.67	1.72	1.72	1.62	1.65
O(2)-*T*(2)-O(3)	109.1(3)	O(2)-*T*(2)-O(3)	110(1)	107(1)	106(1)	110(1)	107.2(8)
O(2)-*T*(2)-O(3)'	112.6(3)	O(2)-*T*(2)-O(4)	114(1)	111(1)	112(1)	113(1)	116(1)
O(2)-*T*(2)-O(4)	104.2(3)	O(2)-*T*(2)-O(5)	103(1)	106(1)	105(1)	102(1)	103.9(8)
O(3)-*T*(2)-O(3)'	112.6(3)	O(3)-*T*(2)-O(4)	113(2)	111(1)	112(1)	113(1)	113(1)
O(3)-*T*(2)-O(4)	110.3(2)	O(3)-*T*(2)-O(5)	109(2)	113(1)	112(1)	110(1)	110(1)
O(3)-*T*(2)-O(4)'	107.7(3)	O(4)-*T*(2)-O(5)	108(2)	108(1)	108(1)	107(1)	107(1)
<O-*T*-O>	109.4		110	109	109	109	109
		T(3) - O(2)	1.67(4)	1.63(3)	1.61(3)	1.73(3)	1.59(2)
		T(3) - O(3)	1.66(3)	1.59(3)	1.60(2)	1.69(2)	1.75(2)
		T(3) - O(4)	1.67(3)	1.60(3)	1.62(2)	1.75(2)	1.76(2)
		T(3) - O(6)	1.67(3)	1.66(3)	1.67(3)	1.76(2)	1.70(2)
		<*T*(3)-O>	1.67	1.62	1.63	1.73	1.70
		O(2)-*T*(3)-O(3)	111(1)	115(1)	116(1)	113(1)	112.4(9)
		O(2)-*T*(3)-O(4)	108(1)	110(1)	108(1)	107(1)	108.0(9)
		O(3)-*T*(3)-O(6)	105(1)	102(2)	103(1)	104(1)	103.8(8)
		O(3)-*T*(3)-O(4)	114(2)	111(1)	113(1)	113(1)	112(1)
		O(3)-*T*(3)-O(6)	107(2)	108(1)	107(1)	107(2)	106.1(9)
		O(4)-*T*(3)-O(6)	112(2)	109(1)	109(1)	111(1)	115(1)
		<O-*T*-O>	110	109	109	109	110
M - O(2)	2.382(7)	*M* - O(2)	2.382(7)	2.36(1)	2.368(8)	2.345(8)	2.361(8)
M - O(3)	2.545(6)	*M* - O(3)	2.55(4)	2.51(3)	2.50(2)	2.55(2)	2.52(2)
M - O(3)	2.545(6)	*M* - O(4)	2.53(3)	2.58(3)	2.56(2)	2.49(2)	2.53(2)
M - O(4)	2.885(5)	*M* - O(5)	2.84(4)	3.01(3)	2.94(2)	2.89(2)	2.85(2)
M - O(4)	2.885(5)	*M* - O(5)'	2.93(3)	2.92(3)	2.88(2)	2.88(2)	2.90(2)
M - O(4)'	2.905(5)	*M* - O(6)	2.88(3)	2.92(2)	2.89(2)	2.76(2)	2.74(2)
M - O(4)'	2.905(5)	*M* - O(6)'	2.93(4)	2.80(3)	2.83(2)	2.85(2)	2.89(2)
<*M*-O>	2.722		2.72	2.73	2.71	2.68	2.68
M - A	2.979(5)		2.98(3)	3.00(3)	3.02(2)	3.09(1)	3.10(1)
M - O(7)	2.322		2.32	2.46	2.35	2.40	2.40
M - O(8)	2.474		2.47	2.38	2.52	2.60	2.60
M - O(9)	2.890		2.89	3.01	2.92	2.98	2.98
M - O(10)	2.370		2.48	2.47	2.42	2.38	2.50
T(1)-O(1)-*T*(1)'	159.3(4)	*T*(1)-O(1)-*T*(1)'	158.6(4)	158.5(5)	160.8(4)	159.6(1)	158.3(4)
T(1)-O(2)-*T*(2)'	140.1(2)	*T*(2)-O(2)-*T*(3)	140(1)	139(1)	140(1)	138(1)	139.0(9)
T(2)-O(3)-*T*(2)'	149.3(3)	*T*(2)-O(3)-*T*(3)	149(2)	149(1)	148(1)	149(1)	147(1)
T(1)-O(4)-*T*(2)	137.4(2)	*T*(2)-O(4)-*T*(3)	149(2)	149(1)	148(1)	144(1)	145(1)
		T(1)-O(5)-*T*(2)	136(1)	140(1)	138(1)	138(1)	137.3(9)
		T(1)-O(6)-*T*(3)	138(1)	138(1)	138(1)	136(1)	136.7(9)
<*T*-O-*T*>	146.5	<*T*(1)-O-*T*>	147.8	148.8	149.4	148.3	147.7
		<*T*(2)-O-*T*>	143.5	144.3	143.5	142.3	142.0
		<*T*(3)-O-*T*>	144.0	143.8	143.5	141.8	141.9

the *A*-cage models proposed by Aitken *et al.* (1984) and Peterson *et al.* (1979).

The variations in the angles O–*T*(1)–O are between 1 and 4°, whereas for O–*T*(2)–O and O–*T*(3)–O they are from 8 to 10°, showing the $T(1)O_4$ tetrahedra to be more symmetrical than the $T(2)O_4$ or $T(3)O_4$ tetrahedra. There does not appear to be any systematic change in angular distortion of the tetrahedra with Al content.

T–O–*T* bond angles are oriented either along the *c* axis or along the *a* axes. The bond angles are very different for the two orientations: about 139° along the *c* axis and 150–160° along the *a* axes. According to Liebau (1985), stressed Si–O–Si bonds, which are energetically unfavorable, are characterized by angles of 139°, whereas unstressed bonds have typical Si–O–Si angles of 160°. There seems to be a linear trend between Al content and the cell parameters *a* and *V* for the five samples of intermediate scapolite ($3.6 < Al < 4.7$) (Table 2). This trend is in agreement with the trend found by Teertstra & Sherriff (1996). As stressed bonds are more flexible than unstressed ones, this difference in mean angle may explain why the *a* cell parameter increases linearly with Al content from 12.04 Å for PAM–4 (3.66 *apfu* Al) to 12.12 Å for MIN (4.53 *apfu* Al), whereas *c* shows only a minor reduction, from 7.58 to 7.57 Å, for the same compositions (Table 2).

Difference Fourier maps (00*z*) were calculated with a 0.02 step along the *c* axis to look for additional volatile species similar to those found in samples PAM–1, PAM–2 and PAM–3 (Sokolova *et al.* 1996). Additional intensity was found only for sample PAM–4 (Fig. 2) where it was confined to the position (00*z*) in the large channels of the structure above and below the *A* site. The numbers on the map indicate the *z* value for the maxima, which are interpreted as being due to the partial occupancy of these channel sites by volatile species.

^{29}Si MAS NMR spectroscopy

^{29}Si MAS NMR spectra for the five samples of scapolite used for Rietveld refinement (PAM–4, TANZ, PAM–5, MAD and MIN), and for the two additional samples used in the ^{27}Al SATRAS experiment (PAM–22 and CA63A), are shown in Figure 3. The similarity of the Al–Si order of PAM–4 and PAM–22, and of PAM–5 and CA63A, is shown by the lack of significant difference between the ^{29}Si MAS spectra for each pair of samples.

The major peaks in all the ^{29}Si MAS NMR spectra of the samples of intermediate scapolite occur at –92 and –106 ppm (Table 5, Fig. 3). These resonances have previously been interpreted as being due to *T*(2,3) (1Si3Al) and *T*(1)(3Si1Al) configurations, respectively (Sherriff *et al.* 1987). The terminology *T*(2,3) is used here; although *T*(2) and *T*(3) are spatially distinct by XRD, they are apparently magnetically equivalent, and it is therefore not possible to distinguish between the sites by MAS NMR spectroscopy. In the spectrum of CA63A (Fig. 3e), with 3.99 Al *apfu*, these are the only peaks, and they have equal intensity, suggesting that this

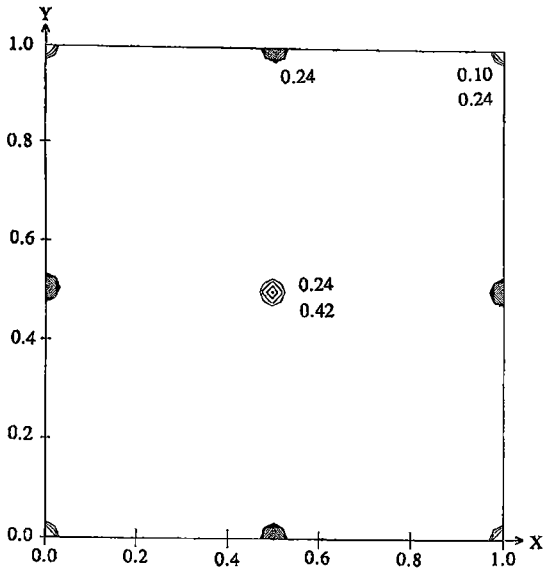

FIG. 2. Difference electron-density maps D(00*z*) for ($0 < z < 0.5$) for PAM–4. The numbers on the maps indicate the *z* value for each maximum.

TABLE 5. ^{29}Si MAS NMR CHEMICAL SHIFTS (PPM) AND RELATIVE INTENSITIES EXPRESSED AS NUMBER OF Si ATOMS

Peak Allocation	PAM-4	PAM-22	TANZ	PAM-5	CA63A	MAD	MIN
T(2,3)(4Al)				-88 0.1 Si		-86 0.2 Si	-86 0.4 Si
T(2,3)(1Si3Al)	-92.4 2.2 Si	-92.4 2.2 Si	-91.7 3.2 Si	-91.8 3.9 Si	-92.0 4.0 Si	-91.7 3.7 Si	-91.3 3.6 Si
T(2,3)(2Si2Al)	-95.5 1.0 Si	-95.5 1.0 Si	-96 0.3 Si				
T(2,3)(3Si1Al)	-98.5 0.7 Si	-98.5 0.7 Si	-98 0.4 Si				
T(2,3)(4Si)	-102.5 -102.5 0.4 Si	-102 0.4 Si	0.3 Si				
*T*1(1Si3Al)						-101.5 0.7 Si	-100.5 1.3 Si
*T*1(3Si1Al)	-106.2 3.0 Si	-106.2 3.0 Si	-105.6 3.5 Si	-106.0 4.0 Si	106.2 4.0 Si	-105.8 3.1 Si	-105.9 2.2 Si
*T*1(4Si)	-110 1.0 Si	-110 1.0 Si	-110 0.4 Si				
Total *T*(2)	4.3 Si	4.3 Si	4.2 Si	4.1 Si	4.0Si	3.9 Si	4.0 Si
Total *T*(1)	4.0 Si	4.0Si	3.9 Si	4.0 Si	4.0 Si	3.8 Si	3.5 Si
Al-O-Al bonds/Al[1]	0.6	0.6	0.3	0.0	0.0	0.0	0.2

(1) number of bonds *pfu* calculated from equation (1)

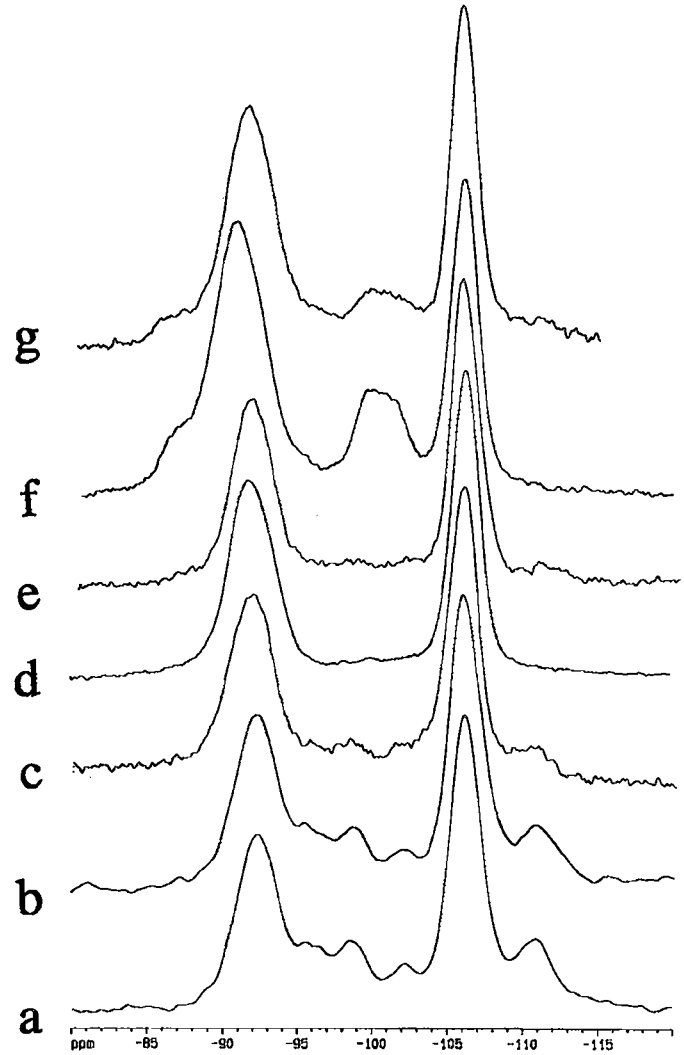

FIG. 3. ^{29}Si MAS NMR spectra of (a) PAM–4, (b) PAM–22, (c) TANZ, (d) PAM–5, (e) CA63A, (f) MAD, and (g) MIN.

sample has a perfectly ordered structure, with Si in the *T*(1) and *T*(3) sites and Al in the *T*(2) site. This composition coincides with the largest difference between mean <*T*(2)–O> and <*T*(3)–O> distances from structural refinements (Table 4; *cf.* Fig. 6, Teertstra & Sherriff 1996). The fact that these peaks remain the dominant peaks in all the spectra in this study shows that the ordered structure is predominant in the intermediate range of scapolite compositions.

PAM–5 (3.90 Al *apfu*) is close in composition to the theoretically perfectly ordered structure at $Al_4Si_8O_{24}$. However, there is a small amount of resonance intensity at –111 ppm (Fig. 3d) in the region allocated to the *T*(1)(4Si) configuration (Sokolova *et al.* 1996). Calculations from the relative intensities of the peaks in the spectral simulations give values of 0.1 Si in the *T*(1)(4Si) environment, 3.9 Si in *T*(3)(3Al1Si), and 4.0 Si in *T*(1)(3Si1Al).

The ^{29}Si MAS NMR spectra of the samples PAM–4, PAM–22 and TANZ, which contain less than 4 Al *apfu*, have additional peaks at about –96, –98, –102 and –111 ppm (Figs. 3a, b, c). These peaks, which decrease in intensity with Al content, have previously been allocated to *T*(2,3)(2Si2Al), *T*(2,3)(3Si1Al), *T*(2,3)(4Si), and

T(1)(4Si) environments, respectively (Sokolova *et al.* 1996); the same interpretation is applied here. If the spectra of PAM–4 and PAM–22 are compared with marialitic samples with Al > 3.25 *apfu* (Sokolova *et al.* 1996), it can be seen that all the peaks become broader with increasing Al content, and spectral simulations show that the *T*(2,3)(2Si2Al) peak can be separately resolved into two peaks of nearly equal intensity at –95.5 and –96.5 ppm. Sherriff *et al.* (1987) reasoned that the effect of replacing Na by Ca in the cavity could cause a change of about 1 ppm in the chemical shift of the adjacent Si atom. Therefore, the peak at –95.5 ppm is allocated to Si in *T*(2,3)(2Si2Al) adjacent to Na, and –96.5 ppm for the same site adjacent to Ca. The increasing peak-width of the peaks at –98, –102 and –111 ppm may also be attributed to the replacement of Na by Ca in the adjacent *M*-sites. The powdered TANZ sample also has a small amount of contamination by albite, which might contribute minor intensity at –92, –97 and –104 ppm (Sherriff & Hartman 1985), possibly overlapping with the scapolite peaks.

For samples PAM–4, PAM–22, TANZ, PAM–5, and CA63A, with 3.66, 3.69, 3.83, 3.90 and 3.99 Al *apfu*, the total amount of Si in the *T*(1) site, calculated from the relative intensity of the ^{29}Si peak, is 4.0 ± 0.1 atoms (Table 5). This corroborates the interpretation of *T*(1)–O bond distances from the Rietveld structure refinements, that there is no Al at the *T*(1) site if the Al content is less than 4 *apfu*.

In the spectra of samples MAD and MIN, there are additional peaks at –88 and –101 ppm, which increase in intensity with increasing Al content from MAD (4.24 *apfu* Al) to MIN (4.53 *apfu* Al). These are allocated, respectively, to *T*(2,3)(4Al) and *T*(1)(2Si2Al) environments caused by Al entering the *T*(1) site (Sherriff *et al.* 1987). Both of these peaks are so broad that the –88 ppm peak overlaps the –92 ppm peak, and the *T*(1)(2Si2Al) peak at –101 ppm can be simulated by several narrow peaks (Fig. 4). The breadth of these peaks is interpreted as being due to multiple peaks related to variations in the type of adjacent alkali cation at the *M* site and also of the anion at the *A* site. There is a shift to low field with decreasing Si content, from PAM–4 to MIN, of 1.1 ppm for the *T*(2,3)(1Si3Al) peak at –92 ppm and of 0.3 ppm for the *T*(1)(3Si1Al) peak at –106 ppm. This shift could be due to a decrease in the ratio of Si to Al in the second coordination shell of *T* atoms. The total amount of Si in the *T*(2,3) site decreases from 4.3 to 4.0 *apfu*, and then remains constant even with increasing total Al *apfu*. Therefore, with Al ≈ 4.0 *apfu*, the *T*(2,3) site always contains 50% Al and 50% Si, with additional Al entering the *T*(1) site.

The number of Al–O–Al bonds per Al atom can be calculated from the relative intensities of the peaks fitted to each ^{29}Si spectrum by using the formula

$$\text{Al–O–Al} = 4 - (\Sigma^{4}_{m=0}\, m\, I_{4,m}/\text{Al}) \qquad (1)$$

modified from Engelhardt & Michel (1987). I is the intensity of the ^{29}Si peak, m is the number of Al atoms in the first coordination shell of *T* atoms, and Al is the number of Al atoms per unit cell.

If this calculation is done for the marialite-rich samples of intermediate scapolite, the result for PAM–4, PAM–22 and TANZ are 0.6, 0.6 and 0.3 Al–O–Al bonds *pfu*, respectively, similar to the values of 0.6, 0.8 and 0.7 reported for the marialite samples PAM–1, PAM–2 and PAM–3 (Sokolova *et al.* 1996). In these compositions of scapolite, Al forms Al–O–Al bonds in spite of the presence of sufficient Si to prevent the violation of Lowenstein's rule (Lowenstein 1954). For PAM–5, CA63A and MAD, this calculation does not show any Al–O–Al bonds in the structures. However, the calculation for MIN gives 0.2 Al–O–Al bonds per Al atom, indicating that with Al ≈ 4, as Al enters *T*(1), Al–O–Al bonds are again formed.

^{27}Al SATRAS NMR spectroscopy

The central transitions (CT) of the ^{27}Al MAS NMR spectra of scapolite show an increase in width with Al content (Fig. 5a; Sherriff *et al.* 1987), but the peaks are asymmetrical, broad and featureless, thus limiting the information that can be extracted. However, the spinning sidebands of the satellite transitions (ST) resolve more fine structure, as the second-order quadrupolar broadening is further reduced compared to the CT. This is the basis of satellite transition (SATRAS) spectroscopy. The third sideband out of the manifold of spinning sidebands is shown in Figure 5b, and stack plots of these ST spinning sidebands are given beneath (Fig. 5c).

It can be seen from plots of the ST that there are up to three different resonances; Peak 1 at 60 ppm, Peak 2 at 63 ppm, and Peak 3 at 67 ppm (Fig. 5b). These values are not true chemical shifts, as the peak positions must be corrected for the second-order quadrupolar shift. Peak 1, present in all the spectra of intermediate scapolite, is equivalent to the single resonance found for PAM–1 (Sokolova *et al.* 1996). Peak 2 is present in all the samples, but increases in intensity with Al content. For the samples of scapolite with an Al > 4, the satellite transitions confirm the presence of at least one other peak, Peak 3 at 67 ppm. This third peak is readily visible in the spinning sidebands of the satellite transitions for samples MIN and MAD (Fig. 5c4 and c5). In order to assign the peaks to site environments, it is necessary to determine the quadrupole parameters, not only to determine the values of the true isotropic chemical shift, but also to gain information concerning site distortion. The quadrupolar coupling constant C_Q, 1.98 MHz, and an asymmetry parameter η, 0.8 to 1.0, were calculated for Peak 1 by fitting the shape of the center band and the sideband, as well as the sideband envelope for the single peak in the spectrum of PAM–1 (Sokolova *et al.* 1996).

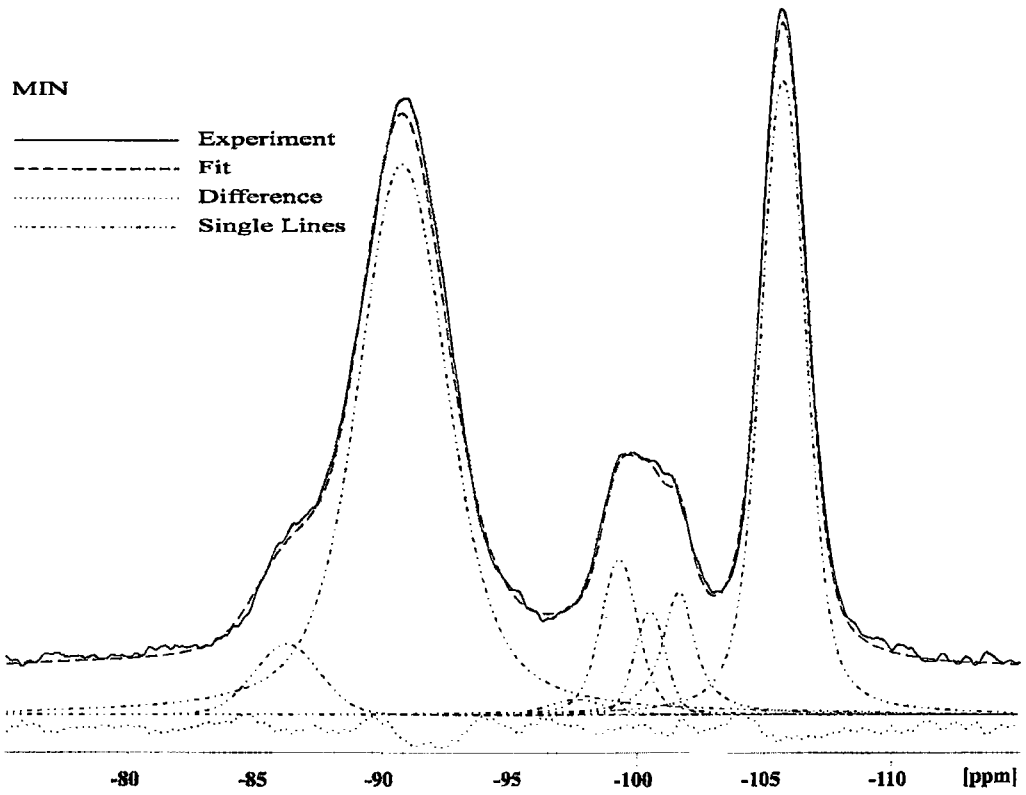

FIG. 4. ^{29}Si MAS NMR spectra of MIN, with six peaks fitted by the least-squares iterative process; the experimental spectrum, fitted peaks and envelope, and the difference between fitted and experimental spectra are shown.

The parameters of the second Al-site were determined on CA63A by deconvoluting the first 42 spinning sidebands of the corrected spectrum (Kunath *et al.* 1992) into two Gaussian lines and simulating both ST-envelopes. The quadrupolar coupling constant C_Q, 3.67–4.33 MHz, and an asymmetry parameter η, 0 to 1.0, were then calculated for Peak 2 by subtracting the spectrum of the 60 ppm peak and fitting the remaining shape of the center band and sideband, and the sideband envelope. The values of C_Q and η could then be used to calculate the second-order quadrupolar shift of the CT and hence the true isotropic chemical shift (δ_{iso}) of Peaks 1 and 2 for each sample of scapolite. However, Peak 3 was not sufficiently resolved for the exact determination of the quadrupolar parameters by this method. However, the relative intensities of the three peaks for intermediate scapolite could be calculated from the spectral simulations. In Table 6, the number of Al in *apfu* represented by each peak is given with the isotropic chemical shifts for Peaks 1 and 2 and the peak position for Peak 3 for PAM–22, TANZ, CA63A, MAD and MIN.

TABLE 6. ^{27}Al SATRAS ISOTROPIC CHEMICAL SHIFTS, AND RELATIVE INTENSITIES EXPRESSED AS NUMBER OF Al ATOMS IN SITE

Site	PAM-22	TANZ	CA63A	MAD	MIN
Peak 1	59.0 ppm 2.7 Al	58.6 ppm 2.6 Al	58.3 ppm 1.9 Al	58.3 ppm 1.7 Al	57.7 ppm 0.8 Al
Peak 2	62.3 ppm 1.0 Al	62.0 ppm 1.2 Al	61.2 ppm 1.9 Al	61.2 ppm 2.2 Al	60.5 ppm 3.3 Al
Peak 3 *T*(1)(3Si1Al)			*65.8 ppm 0.2 Al	*66.4 ppm 0.3 Al	*67.1 ppm 0.4 Al
**T(1)	54.1 ppm	53.3 ppm	52.9 ppm	53.7 ppm	54.2 ppm
**T(2)	57.4 ppm	56.8 ppm	57.4 ppm	58.3 ppm	58.6 ppm
**T(3)	57.0 ppm	57.2 ppm	57.4 ppm	58.7 ppm	58.6 ppm

* Peak Position not isotropic chemical shift
** δ_{iso} calculated from $\delta_{iso} = -0.77\,\theta + 167.9$ (Phillips *et al.* 1989).

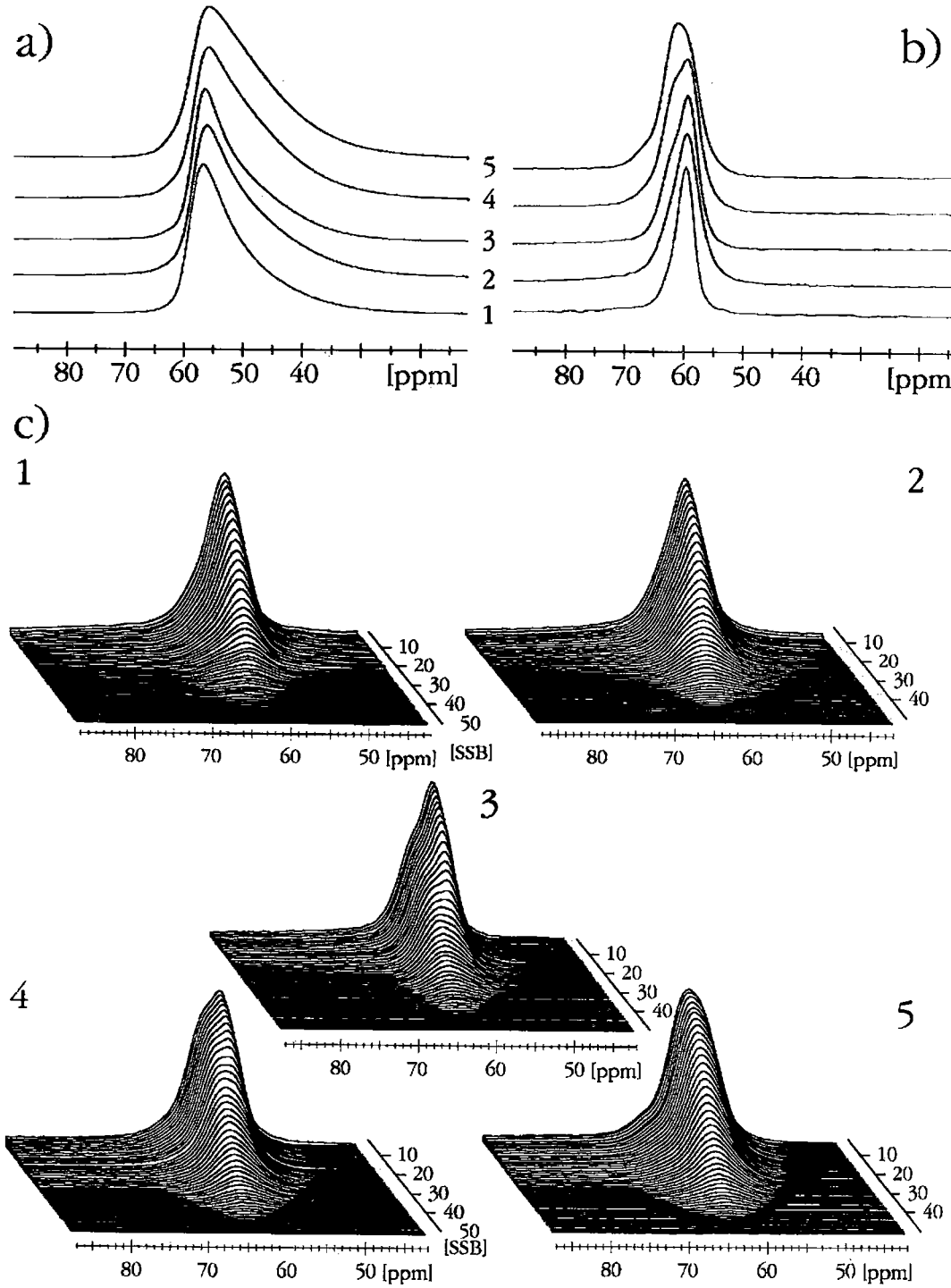

FIG. 5. ^{27}Al satellite transition spectra of (1) PAM–22, (2) TANZ, (3) CA63A, (4) MAD, and (5) MIN showing (a) the central transition, (b) satellite transition line-shape, (c) stack plots 1 – 5 of the ST spinning sidebands.

Interpretation of the ^{27}Al MAS NMR spectra of scapolite is not as straightforward as for ^{29}Si MAS NMR. For groups of silicate minerals with similar structures, ^{29}Si isotropic chemical shift has been correlated with changes in Si–O–*T* bond angle and Si–O bond length (Higgins & Woessner 1982, Smith *et al.* 1983, Smith & Blackwell 1983, Engelhardt & Radeglia 1984, Radeglia and Engelhardt 1985), and with the electronegativity of neighboring cations (Mägi *et al.* 1984, Grimmer & Radeglia 1984, Janes & Oldfield 1985). Sherriff and coworkers found that the chemical shift for all aluminosilicate minerals could be correlated to the position and bond valence of neighboring cations (Sherriff & Grundy 1988, Sherriff *et al.* 1991). In the spectra of scapolite, ^{29}Si peaks can be interpreted in terms of different combinations of Si and Al neighbors around the *T*(1) and *T*(2,3) sites, with additional divisions of peaks relating to the type of adjacent alkali cation (Sherriff *et al.* 1987). If similar factors are responsible for the variations in the ^{27}Al chemical shift at tetrahedral sites in aluminosilicate minerals, and if Lowenstein's Rule is obeyed, there should be a single peak for scapolite with Al < 4 representing Al in the *T*(2,3)(4Si) environment. With Al > 4, two extra peaks should appear due to Al in *T*(2,3)(3Si1Al) and *T*(1)(3Si,1Al) environments as Al enters the *T*(1) site, which would increase in intensity relative to the first peak with Al content. It was clear, even from early work using poorly resolved MAS spectra (Sherriff *et al.* 1987), that this was not the case, as the broad peak was found to increase progressively in width with increasing Al content. In the structure of scapolite with Al-poor compositions, the calculation from the ^{29}Si spectra of up to 80% of Al being involved in one Al–O–Al bond makes the picture more complex, as it would produce a single peak for Al = 4 and extra peaks for samples with either more or less Al.

Peak 3, at 67 ppm, is assigned to Al in the *T*(1) site, as it is present only in samples with Al ≈ 4, and increases in relative intensity with Al content. The minor intensity of Peak 3 in the spectrum of CA63A shows the first evidence of Al entering the *T*(1) site at Al = 4 *apfu*, contrary to the interpretation of XRD and ^{29}Si MAS NMR results. Once Al enters the *T*(1) site, there must be Al–O–Al bonds involving *T*(1), and therefore Peak 3 is assigned to the T(1)(3Si1Al) environment.

Peak 1 ($59.0 < \delta_{iso} < 57.7$ ppm; $C_Q = 1.98$ MHz; $0.8 < \eta < 1.0$) and Peak 2 ($62.3 < \delta_{iso} < 60.5$ ppm; $3.67 < C_Q < 4.33$ MHz; $0.0 < \eta < 1.0$) is assigned to Al in the *T*(2,3) site, as both XRD and ^{29}Si MAS NMR show Al only in the *T*(2,3) sites with Al < 4. If the greatest effect on the ^{27}Al chemical shift of Q^4 sites in aluminosilicates is dependent upon the identity of the neighboring tetrahedrally coordinated atom (whether Si or Al), as is found for the corresponding ^{29}Si chemical shifts (Lippmaa *et al.* 1980, 1981, Mägi *et al.* 1984), then Peak 1 would be due to *T*(2,3)(3Si1Al), and Peak 2, to *T*(2,3)(4Si). However, Peak 1 makes up 50% of the total intensity for sample CA63A, for which the ^{29}Si spectrum shows no evidence of Al–O–Al bonds; in fact, the presence of Al–O–Al bonds would contradict the XRD-based structural evidence for a high degree of Al–Si order at this composition.

^{27}Al isotropic chemical shifts have been correlated with the number of neighboring tetrahedrally coordinated atoms (Bradley *et al.* 1993, and references therein), but owing to an assumption that Lowenstein's Rule is always obeyed, correlations have not been made with replacement of next-nearest neighbor (NNN) Si by Al. Tossell (1993) calculated that the difference in energy between paired and alternating Si and Al atoms in a four-membered ring of $Si_2Al_2O_{12}H_8^{2-}$ is only 63 kJ/mol rather than the previously calculated values of >400 kJ/mol (Hass *et al.* 1981, Sauer & Engelhardt 1982, Navrotski *et al.* 1985, Derouane *et al.* 1990, Pelmenschikov *et al.* 1992). This value is further reduced by about 22 kJ/mol by the addition of a single Na cation to the atom of bridging oxygen, as is present in the structure of marialite-rich scapolite. This 40 kJ/mol result is consistent with the calorimetric data of Navrotski *et al.* (1982, 1985) and calculated values for lattice-energy minimization (Bell *et al.* 1992). Therefore Al(3Si1Al) sites may be more common in aluminosilicates structures than anticipated in earlier interpretations of ^{27}Al spectra.

Linear relationships between ^{27}Al isotropic chemical shift of tetrahedral sites in aluminosilicate structures and mean Al–O–Si bond angle give different correlations for ordered (Phillips *et al.* 1989) and disordered structures (Lippmaa *et al.* 1986). This difference is due to the increased mean Al–O–Si bond angles in disordered structures compared to ordered structures, *e.g.*, feldspar or leucite (Kirkpatrick & Phillips 1993). In the ordered structure of scapolite (Al = 4), the *T*(3) site is fully occupied by Al. Therefore, the correlation for the ordered aluminosilicate structures (Phillips *et al.*1989) is given by

$$\delta_{iso} = -0.77\ \theta + 167.9 \qquad (2)$$

where θ is the mean Al–O–T angle. Equation 2 was used to calculate a value of δ_{iso} of 57.4 ppm for *T*(3) site for the ordered structure of PAM–5. However, the mean *T*–O–*T* angles for *T*(2) and *T*(3) are both 143.5° despite the presence of Si at *T*(2), and of Al at *T*(3). Therefore, the replacement of Si by Al in the *T*(2,3) site does not seem to affect the *T*–O–*T* angles, and it is not surprising that Al(4Si) and Al(3Si1Al) sites have the same chemical shift.

A minor change in <*T*(2,3)–O–*T*> angle with increasing Al content, from 144° for PAM–4 to 142° for MIN, results in an increase in the calculated δ_{iso} of about 1 ppm across the series for both *T*(2) and *T*(3) (Table 6). As this increase in δ_{iso} is apparently not correlated with Al replacing Si as next-nearest-neighbor, it must be related to the identity of the alkali cation or

anion in the *M* or *A* sites. As the mean bond angle is constant for the marialite samples in which Ca replaces Na at the *M* site but only Cl is found in the *A* site (Sokolova *et al.* 1996), it is more likely that this change in bond angle (and hence in chemical shift) is related, in intermediate-range scapolite, to the presence of either Cl or CO_3 at the *A* site.

To investigate empirically the possible cause of the two *T*(2,3) ^{27}Al peaks, the relative intensity of Peak 1 (calculated as a percentage of the sum of the intensities of Peaks 1 and 2) was plotted against (i) the percentage of *T*(2,3) atoms involved in Al–O–Al linkages (Fig. 6a), (ii) the percentage of Na at the *M* site (Fig. 6b), and (iii) the percentage Cl at the *A* site (Fig. 6c). The correlation coefficients (r) for the three plots are 0.830, 0.987 and 0.993, respectively, showing that there is a much stronger correlation between the amount of Al in *T*(2,3) represented by Peak 1 and the occupancy of the *M* and *A* sites than with the possibility of Al–O–Al bonds. Therefore, it seems that the difference between the Al sites that contribute to Peak 1 and Peak 2 is related to the difference in local symmetry of the *T*(2,3) site, depending on the characteristics of the adjacent anion and alkali or alkaline earth cation. ^{23}Na single-crystal NMR spectra of three samples of scapolite have shown that the symmetry of the Na electric-field gradient is strongly affected by the type of adjacent anion (Sherriff & Kunath-Fandrei, in prep). Information about changes at the anion site could be transmitted through the electric field gradient at the *M* site to Al in the adjacent *T*(2,3) site. Peak 1 is therefore assigned to *T*(2,3) site adjacent to Na, and Peak 2, to *T*(2,3) adjacent to Ca.

Conclusions

Rietveld refinements from X-ray powder data of intermediate samples in the scapolite series with 3.66 ≤ Al ≤ 4.53 *apfu* revealed information about the population of the *T*(2,3) sites on the basis of the interatomic <*T*–O> distances. Tetragonal symmetry described by space group *I*4/*m* is preferable for PAM–4, and space group $P4_2/n$, for TANZ, PAM–5, MAD, and MIN. Structural differences between the space groups do not refer to the *M* and *A* sites, as the choice of space group is determined only by the degree of order of Si and Al in the tetrahedral sites. Space group $P4_2/n$ corresponds to the ordered Al–Si distribution over the *T* sites of the scapolite framework. With variation in Al from 3.66 to 4.53 *apfu*, there is a linear increase in *a* from 12.04 to 12.12 Å, although the *c* unit-cell dimension remains almost constant. The increase is closely related to the variation of *T*–O–*T* angles parallel to *a*.

The relative intensities of the peaks in the ^{29}Si MAS and ^{27}Al SATRAS NMR spectra agree with the general interpretation of Al–Si order from the structural refinements, but also contribute further information about short-range order. The ^{27}Al SATRAS and ^{29}Si MAS NMR spectra of intermediate-range scapolite show that

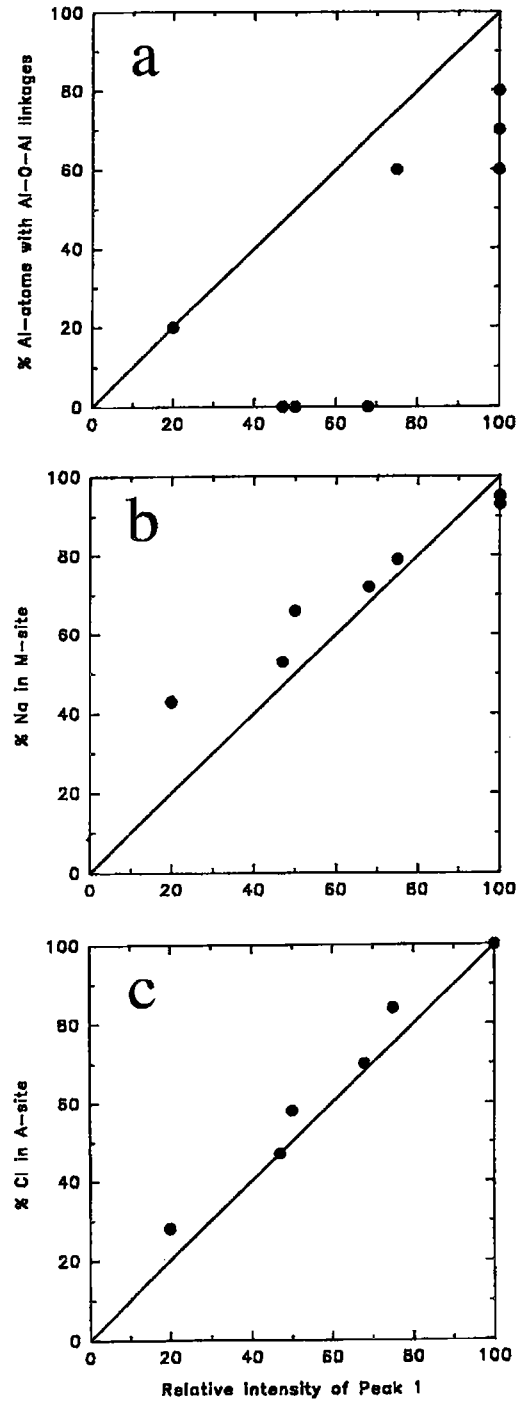

FIG. 6. The intensity of ^{27}Al SATRAS NMR Peak 1, plotted as a percentage of the total intensity of Peaks 1 and 2, *versus* the percentage of (a) *T*(2,3) atoms involved in Al–O–Al linkages, (b) alkali sites containing Na, and (c) anion sites containing Cl.

Al enters the $T(1)$ site only where there are more than 4 Al *apfu*, in agreement with the Rietveld structure refinement. The ^{29}Si spectra show an ordered structure for scapolite with Al near 4 *apfu*, but with Al–Si disorder being introduced and Al–O–Al bonds being formed as Al becomes progressively greater or lesser than 4.

The ^{27}Al SATRAS spectra are apparently more sensitive than ^{29}Si MAS spectra to site distortion. They reveal a difference in symmetry of the $T(2,3)$ site that is related to the type of population of the alkali cation and anion sites. They also show that a small amount of Al can enter the $T(1)$ site in the ordered structure with Al equal to 4 *apfu*, an amount that can be undetected by XRD or ^{29}Si MAS NMR.

Acknowledgements

Samples were kindly provided by D. Shaw, D. Moecher, S. Sergeev and F. Rafikova. Research expenses were supported by Russian Fund for Basic Research grant 97-05-64000 to EVS and YKK, a Natural Sciences and Engineering Research Council University Research Fellowship and Research Grant to BLS. We also thank two anonymous reviewers for helpful comments.

References

Aitken, B.G., Evans, H.T., Jr. & Konnert, J.A. (1984): The crystal structure of a synthetic meionite. *Neues Jahrb. Mineral., Abh.* **149**, 309-342.

Bell, R.G., Jackson, R.A. & Catlow, C.R.A. (1992): Lowenstein's rule in Zeolite-A: a computational study. *Zeolites* **12**, 870-871.

Belokoneva, E.L., Sokolova, N.V. & Dorokhova, G.I. (1991): Crystal structure of natural Na,Ca-scapolite – an intermediate member of the marialite – meionite series. *Sov. Phys. Crystallogr.* **36**, 828-830.

_____, _____ & Urusov, V.S. (1993): Scapolite – crystalline structures of marialite (Me_{11}) and meionite (Me_{88}) – space group as a function of composition. *Crystallogr. Reports* **38**(1), 25-28 (translated from *Kristallogr.* **38**, 52-77).

Berar, J.-F. & Lelann, P. (1991): E.S.D's and estimated probable error obtained in Rietveld refinements with local correlations. *J. Appl. Crystallogr.* **24**, 1-5.

Bradley, S.M., Howe, R.F. & Kydd, R.A. (1993): Correlation between ^{27}Al and ^{71}Ga NMR chemical shifts. *Magn. Reson. Chem.* **31**, 883-886.

Comodi, P., Mellini, M. & Zanazzi, P.F. (1990): Scapolites: variation of structure with pressure and possible role in the storage of fluids. *Eur. J. Mineral.* **2**, 195-202.

Coolen, J.J.M.M.M. (1980): Chemical petrology of the Furua granulite complex, southern Tanzania. *GUA Papers Geology (Univ. Amsterdam)*, 1-258.

Derouane, E.G., Fripiat, J.G. & Ballmoos, R. (1990): Quantum mechanical calculations on molecular sieves. II. Model cluster investigation of silico-alumino-phosphates. *J. Phys. Chem.* **94**, 1687-1692.

Dunn, P.J., Nelen, J.E. & Norberg, J. (1978): On the composition of gem scapolites. *J. Gemmol.* **16**, 4-10.

Engelhardt, G. & Michel, D. (1987): *High Resolution Solid-State NMR of Silicates and Zeolites.* John Wiley and Sons, New York, N.Y.

_____ & Radeglia, R. (1984): A semi-empirical quantum-chemical rationalization of the correlation between SiOSi angles and ^{29}Si NMR chemical shifts of silica polymorphs and framework aluminosilicates (zeolites). *Chem. Phys. Lett.* **108**, 271-274.

Evans, B.W., Shaw, D.M. & Haughton, D.R. (1969): Scapolite stoichiometry. *Contrib. Mineral. Petrol.* **24**, 293-305.

Grimmer, A.-R. & Radeglia, R. (1984): Correlation between the isotropic ^{29}Si chemical shifts and the mean silicon – oxygen bond lengths in silicates. *Chem. Phys. Lett.* **106**, 262-265.

Hass, E.C., Mezey, P.G. & Plath, P.J. (1981): A non-empirical molecular orbital study on Lowenstein's rule and zeolite composition. *J. Molecular Struct.* **76**, 389-399.

Hassan, I. & Buseck, P.R. (1988): HRTEM characterization of scapolite solid solutions. *Am. Mineral.* **73**, 119-134.

Higgins, J.B. & Woessner, D.E. (1982): ^{29}Si,^{27}Al, ^{23}Na spectra of framework silicates. *Eos, Trans. Am. Geophys. Union* **63**, 1139 (abstr.).

Hill, R.G. & Flack, H.D. (1987): The use of the Durbin-Watson d statistic in Rietveld analysis. *J. Appl. Crystallogr.* **20**, 356-361.

Hoefs, J., Coolen, J.J.M.M.M. & Touret, J. (1981): The sulfur and carbon isotope composition of scapolite-rich granulites from southern Tanzania. *Contrib. Mineral. Petrol.* **78**, 332-336.

Janes, N. & Oldfield, E. (1985): Prediction of silicon-29 nuclear magnetic resonance chemical shifts using a group electronegativity approach; applications to silicate and aluminosilicate structures. *J. Am. Chem. Soc.* **107**, 6769-6775.

Jones, A.P., Smith, J.V., Dawson, J.B. & Hansen, E.C. (1983): Metamorphism, partial melting, and K-metasomatism of garnet – scapolite – kyanite granulite xenoliths from Lashaine, Tanzania. *J. Geol.* **91**, 143-165.

Kirkpatrick, R.J. & Phillips, B.L. (1993): ^{27}Al NMR spectroscopy of minerals and related materials. *Appl. Magn. Reson.* **4**, 213-236.

Kunath, G., Losso, P., Steuernagel, S., Schneider, H. & Jäger, C. (1992): ^{27}Al satellite transition spectroscopy (SATRAS) of polycrystalline aluminium borate $9Al_2O_3{\cdot}2B_2O_3$. *Solid State Nuclear Magn. Res.* **1**, 261-266.

LEVIEN, L. & PAPIKE, J.J. (1976): Scapolite crystal chemistry: aluminum – silicon distributions, carbonate group disorder and thermal expansion. *Am. Mineral.* **61**, 864-877.

LIEBAU, F. (1985): *Structural Chemistry of Silicates. Structure, Bonding, and Classification.* Springer-Verlag, Berlin, Germany.

LIN, S.B. (1975): Crystal chemistry and stoichiometry of the scapolite group. *Acta Geol. Taiwanica* **18**, 36-48.

_____ & BURLEY, B.J. (1973a): Crystal structure of a sodium and chlorine-rich scapolite. *Acta Crystallogr.* **B29**, 1272-1278.

_____ & _____ (1973b): On the weak reflections violating body-centered symmetry in scapolites. *Tschermaks Mineral. Petrogr. Mitt.* **20**, 28-44.

_____ & _____ (1973c): The crystal structure of meionite. *Acta Crystallogr.* **B29**, 2024- 2026.

_____ & _____ (1975): The crystal structure of an intermediate scapolite – wernerite. *Acta Crystallogr.* **B31**, 1806-1814.

LIPPMAA, E., MÄGI, M., SAMOSON, A., ENGELHARDT, G. & GRIMMER, A.-R. (1980): Structural studies of silicates by solid-state, high resolution ^{29}Si NMR. *J. Am. Chem. Soc.* **102**, 4889-4893.

_____, _____, _____, TARMACK, M. & ENGELHARDT, G. (1981): Investigation of the structure of zeolites by solid-state, high-resolution ^{29}Si NMR spectroscopy. *J. Am. Chem. Soc.* **103**, 4992-4996.

_____, SAMOSON, A. & MÄGI, M. (1986): High resolution ^{27}Al NMR of aluminosilicates. *J. Am. Chem. Soc.* **108**, 1730-1735.

LOWENSTEIN, W. (1954): The distribution of aluminum in the tetrahedra of silicates and aluminosilicates. *Am. Mineral.* **39**, 92-96.

MÄGI, M., LIPPMAA, E., SAMOSON, A., ENGELHARDT, G. & GRIMMER, A.-R. (1984): Solid state high- resolution silicon-29 chemical shift in silicates. *J. Phys. Chem.* **88**, 1518-1522.

MOECHER, D.P. (1988): *Scapolite Phase Equilibria and Carbon Isotope Variations in High Grade Rocks: Tests of the CO_2-Flooding Hypothesis of Granulite Gneiss.* Ph.D. thesis, Univ. Michigan, Ann Arbor, Michigan.

NAVROTSKI, A., GEISINGER, K.L., MCMILLAN, P. & GIBBS, G.V. (1985): The tetrahedral framework in glasses and melts: inferences from molecular orbital calculations and implications for structure, thermodynamics and physical properties. *Phys. Chem. Minerals* **11**, 284-298.

_____, PERAUDEAU, G., MCMILLAN, P. & COUTURES, J.-P. (1982): A thermochemical study of glasses and crystals along the joins silica-calcium aluminate and silica-sodium aluminate. *Geochim. Cosmochim. Acta* **46**, 2039-2047.

PAPIKE, J.J. & STEPHENSON, N.C. (1966): The crystal structure of mizzonite, a calcium- and carbonate-rich scapolite. *Am. Mineral.* **51**, 1014-1027.

_____ & ZOLTAI, T. (1965): The crystal structure of a marialite scapolite. *Am. Mineral.* **50**, 641- 655.

PELMENSCHIKOV, A.G., PAUKSHTIS, E.A., EDISHERASHVILI, M.O. & ZHIDOMIROV, G.M. (1992): On the Lowenstein's rule and mechanism of zeolite dealumination. *J. Phys. Chem.* **96**, 7051-7055.

PETERSON, R.C., DONNAY, G. & LE PAGE, Y. (1979): Sulfate disorder in scapolite. *Can. Mineral.* **17**, 53-61.

PHILLIPS, B.L., KIRKPATRICK, R.J. & PUTNIS, A. (1989): Si, Al ordering in leucite by high resolution ^{27}Al MAS NMR spectroscopy. *Phys. Chem. Minerals* **16**, 591-598.

POUCHOU, J.-L. & PICHOIR, F. (1985): "PAP" (phi-rho-Z) procedure for improved quantitative microanalysis. *In Microbeam Analysis* (J.T. Armstrong, ed.). San Francisco Press, San Francisco, California (104-106).

RADEGLIA, R. & ENGELHARDT, G. (1985): Correlation of Si–O–T (T = Si or Al) angles and ^{29}Si NMR chemical shifts in silicates and aluminosilicates. Interpretation by semi-empirical quantum-chemical considerations. *Chem. Phys. Lett.* **114**, 28-30.

SAUER, J. & ENGELHARDT, G. (1982): Relative stability of Al–O–Al linkages in zeolites. A non empirical molecular orbital study. *Z. Natur.* **37a**, 277-279.

SCHNEIDER, J. (1989): Profile refinement on IBM-PC's. *I.U. Dr. Int. Workshop on the Rietveld Method.* M. Schneider EDV, Beijing, China.

SHANNON, R.D. & PREWITT, C.T. (1969): Effective ionic radii in oxides and fluorides.*Acta Crystallogr.* **B25**, 925-946.

SHAW, D.M., SCHWARCZ, H.P. & SHEPPARD, S.M.F. (1965): The petrology of two zoned scapolite skarns. *Can. J. Earth Sci.* **2**, 577-595.

SHERRIFF, B.L. & GRUNDY, H.D. (1988): Calculation of ^{29}Si MAS NMR chemical shift from silicate mineral structure. *Nature* **332**, 819-822.

_____, _____ & HARTMAN, J.S. (1987): Occupancy of T-sites in the scapolite series. A multinuclear NMR study using magic-angle spinning. *Can. Mineral.* **25**, 717-730.

_____, _____ & _____ (1991): The relationship between ^{29}Si MAS NMR chemical shift and silicate mineral structure. *Eur. J. Mineral.* **3**, 751-768.

_____ & HARTMAN, J.S. (1985): Solid-state high resolution ^{29}Si NMR of feldspars: Si/Al disorder and the effects of paramagnetics. *Can. Mineral.* **23**, 205-212.

SKIBSTED, J., NIELSON, N.C., BILDSØE, H. & JAKOBSEN, H.J. (1991): Satellite transitions in MAS NMR spectra of quadrupolar nuclei. *J. Magn. Res.* **95**, 88-117.

SMETZER, K., OTTEMANN, J. & KRUPP, H. (1976): Scapolite from central Tanzania. *Aufschluss* **27**, 341-346.

SMITH, J.V. & BLACKWELL, C.S. (1983): Nuclear magnetic resonance of silica polymorphs. *Nature* **303**, 223-225.

SMITH, K.A., KIRKPATRICK, R.J., OLDFIELD, E. & HENDERSON, D.M. (1983): High resolution silicon-29 nuclear magnetic resonance spectroscopic study of rock-forming silicates. *Am. Mineral.* **68**, 1206- 1215.

SOKOLOVA, E.V., KABALOV, Y.K., SHERRIFF, B.L., TEERTSTRA, D.K., JENKINS, D.M., KUNATH-FANDREI, G., GOETZ, S. & JÄGER, C. (1996): Marialite: Rietveld structure-refinement, and ^{29}Si MAS and ^{27}Al satellite transition NMR spectroscopy *Can. Mineral.* **34**, 1039-1051.

TEERTSTRA, D.K. & SHERRIFF, B.L. (1996): Scapolite cell-parameter trends along the solid-solution series. *Am. Mineral.* **81**, 169-180.

_____ & _____ (1997): Substitutional mechanisms, compositional trends and the end member formulae of scapolite. *Chem. Geol.* **136**, 233-260.

TOSSELL, J.A. (1993): A theoretical study of the molecular basis of the Al avoidance rule and of the spectral characteristics of Al–O–Al linkages. *Am. Mineral.* **78**, 911-920.

ULBRICH, H.H. (1973): Structural refinement of the Monte Somma scapolite, a 93% meionite. *Schweiz. Mineral. Petrogr. Mitt.* **53**, 385-393.

ZOLOTAREV, A.A. (1993): Gem scapolite from the eastern Pamirs and some general constitutional features of scapolites. *Zap. Vser. Mineral. Obshchest.* **122**(2), 90-102 (in Russ.).

_____ (1996): Once more about isomorphic schemes and isomorphic series in the scapolite group. *Zap. Vser. Mineral. Obshchest.* **125**(1), 69-73 (in Russ.).

ZWAAN, P.C. (1971): Yellow scapolite, another gem-mineral from Umba, Tanzania. *J. Gemmol.* **12**, 304-309.

Received September 19, 1997, revised manuscript accepted October 19, 1998.